Fourier and the science of today / Fourier et la science d'aujourd'hui

Multivariate scale-free temporal dynamics: From spectral (Fourier) to fractal (wavelet) analysis

Dynamique temporelle multivariée invariante d'échelle : de l'analyse spectrale (Fourier) à l'analyse fractale (ondelette)

Patrice Abry [a],[*], Herwig Wendt [b], Stéphane Jaffard [c], Gustavo Didier [d]

[a] *Université de Lyon, ENS de Lyon, CNRS, Laboratoire de physique, Lyon, France*
[b] *IRIT, CNRS (UMR 5505), Université de Toulouse, France*
[c] *Université Paris-Est, LAMA (UMR 8050), UPEM, UPEC, CNRS, Créteil, France*
[d] *Department of Mathematics, Tulane University, New Orleans, LA, USA*

A B S T R A C T

The Fourier transform (or spectral analysis) has become a universal tool for data analysis in many different real-world applications, notably for the characterization of temporal/spatial dynamics in data. The wavelet transform (or multiscale analysis) can be regarded as tailoring spectral estimation to classes of signals or functions defined by scale-free dynamics. The present contribution first formally reviews these connections in the context of multivariate stationary processes, and second details the ability of the wavelet transform to extend multivariate scale-free temporal dynamics analysis beyond second-order statistics (Fourier spectrum and autocovariance function) to multivariate self-similarity and multivariate multifractality. Illustrations and qualitative discussions of the relevance of scale-free dynamics for macroscopic brain activity description using MEG data are proposed.

© 2019 Académie des sciences. Published by Elsevier Masson SAS. This is an open access article under the CC BY-NC-ND license (http://creativecommons.org/licenses/by-nc-nd/4.0/).

R É S U M É

La transformée de Fourier (ou analyse spectrale) est aujourd'hui devenue un outil universel pour l'analyse de données issues de nombreuses applications réelles de natures très différentes, particulièrement pertinent pour la caractérisation de la dynamique temporelle ou spatiale. La transformée en ondelettes (ou analyse multéchelle) peut être vue comme une analyse spectrale adaptée à des classes de signaux ou fonctions dont la dynamique est invariante d'échelle. La présente contribution propose d'abord de faire un état de l'art des relations formelles entre ces deux analyses dans le cadre des processus aléatoires stationnaires multivariés, puis de montrer la capacité de la transformée en ondelettes à étendre l'analyse de l'invariance d'échelle multivariée au-delà des statistiques de second ordre (fonction de covariance et spectre de Fourier), à l'auto-similarité multivariée et à la multifractalité multivariée. Quelques illustrations et éléments de discussion sur la

---

* Corresponding author.
  E-mail addresses: patrice.abry@ens-lyon.fr (P. Abry), herwig.wendt@irit.fr (H. Wendt), jaffard@u-pec.fr (S. Jaffard), gdidier@tulane.edu (G. Didier).

pertinence de ces concepts et outils pour l'analyse de l'activité cérébrale macroscopique sont proposés.

1. Introduction

1.1. Context: from frequency to scale representations

Fourier (spectral) transform and multivariate temporal dynamics. The Fourier transform has become a universal tool in almost all fields of the sciences. Notably, it has been used to analyze data from numerous real-world applications where the information of interest is conveyed by the multivariate temporal or spatial dynamics of collections of *signals* (*images, fields, flows of images, video…*). Such dynamics are often well accounted for by the so-called Fourier spectrum, defined as the Fourier transform of auto- and cross-covariance functions, which is thus tied to second-order (or two point) statistics of data [1]. Besides countless successes in real-world applications, very different in nature, ranging from natural sciences and engineering to social sciences, the popularity of the Fourier transform relies on a solid mathematical foundation [2–4] and fast and efficient computer implementations (algorithms) [5,6].

Wavelet (multiscale) transform and multivariate scale-free dynamics. The Fourier transform and spectral analysis are documented to be of particular relevance and interest when temporal dynamics are well characterized by oscillatory behavior, corresponding to energy concentration within narrow frequency bands (for example, macroscopic brain activity with well-defined frequency bands known to be associated with brain activity, e.g., the alpha-band and attention… [7]). For such cases, data are well described by mathematical models (Markov processes, ARMA models…) whose definitions are deeply tied to one (or a few) well-defined characteristic scale(s) of time, or equivalently, of frequency ranges. However, the "scale-free paradigm" is observed to be a superior modeling framework for a great number of complex or large-dimensional data sets stemming from a wide range of modern fields of investigation. This includes areas such as human socio-economic activities (Internet traffic [8–11], finance [12–14], geography [15], art investigation [16,17]…) and natural phenomena (heart rate rhythms [18–22], neuroscience [23–26] or hydrodynamic turbulence [27–29] and geophysics [30,31]…). The original intuition into scale-free behavior may likely be traced back to the seminal works of B. Mandelbrot [32–34]: temporal dynamics are governed by a large continuum of time scales, and crucial information is no longer encoded in the identification of one or a few time scales, but rather in the relations amongst time scales [8]. Such situations have been abundantly characterized, notably, by means of conceptual models such as $1/f$-processes, self-similarity and (multi)fractality. Neuroscience provides a rich context of particular interest where scale-free dynamics has been applied to the modeling of infraslow spontaneous macroscopic brain activity [24,35]. It has also prompted the use of the wavelet transform instead of the Fourier transform, that is, of scale-dependent rather than frequency-dependent analysis [36,37]. This was shown to efficiently reformulate spectral analysis, both theoretically and practically [8,10,38–41].

Beyond Fourier and second-order statistics. Multivariate temporal dynamics characterization is naturally grounded in second order statistical analysis (Fourier spectra and auto- and cross- covariances). By contrast, its wavelet counterpart permits extensions that are theoretically well-grounded and efficient in practice to higher order statistics, and also to some forms of non-stationarity [8]. This is accomplished by means of the concepts of multivariate self-similarity [42–44] and multivariate multifractality [45,46].

1.2. Goals, contributions, and outlines: wavelet and higher-order multivariate temporal dynamics

The overall goal of the present contribution is to show the extent to which wavelet transforms encompass and enrich Fourier transforms for the analysis of multivariate scale-free dynamics. Fourier-based and wavelet-based spectral estimation for multivariate stationary stochastic processes are thus reviewed and compared in Section 2. The richness of wavelet eigenspectrum-based analysis for multivariate self-similarity is detailed in Section 3. The need for extending wavelet to wavelet leader analysis in multifractal analysis, together with the interest in multivariate multifractal analysis, is described in Section 4.

A MATLAB toolbox implementing the wavelet-based analysis of scale-free dynamics is publicly and freely available with documentation at http://www.ens-lyon.fr/PHYSIQUE/Equipe3/Multifractal/.

2. Fourier vs. wavelet multivariate spectral estimation

2.1. Fourier-based spectral estimation

2.1.1. Stationary stochastic processes

Let $(X_m(t))_{m=1,\ldots,M, t \in \mathbb{R}}$ be a M-variate, real-valued, finite variance stationary stochastic process, with well-defined auto- and cross-covariance functions, $C_{m,n}(\tau) = \mathbb{E}\left(X_m(t)X_n^*(t+\tau)\right)$, and Fourier (or frequency) spectra, $\Gamma_{m,n}(\nu) = (\mathcal{F}C_{m,n})(\nu)$,

where $\mathbb{E}$ denotes the ensemble average, $*$ denotes complex conjugation, and $\tilde{f}(\nu) = (\mathcal{F}f)(\nu) = \int f(t)\exp(-2i\pi\nu t)\,dt$ is the Fourier transform of f.

2.1.2. Multivariate Fourier-based spectral estimation

Classical nonparametric spectral estimation, often referred to as *periodogram* or *Welch* spectral estimation [1], is grounded in the use of the short-time Fourier (or Gabor) transform (STFT) [47]. The STFT coefficients $g_X(\ell,k)$ are defined by comparing, by means of inner products, the signal to analyze, $X(t)$, against a collection of translated and frequency-shifted templates, $\phi_{\ell,k}(t) = \phi(t - kT_0)\exp(-2i\ell\nu_0 t)$ of a reference pattern $\phi(t)$: $g_X(\ell,k) = \langle X, \phi_{\ell,k}\rangle$. The time and frequency resolutions T_0 and ν_0 are positive quantities that can be arbitrarily chosen, provided that they satisfy $T_0\nu_0 \leq 1/(4\pi)$. Under mild conditions on the finite-energy function $\phi(t)$, the STFT can be inverted, and $g_X(\ell,k)$ can be interpreted as the joint time and frequency content of X around time $t = kT_0$ and frequency $\nu = \ell\nu_0$ [47].

STFT-based multivariate spectral analysis amounts to estimating the frequency spectra $\Gamma_{m,n}(\nu)$ by time averages (thus assuming ergodicity of X, in addition to stationarity) of STFT coefficients squared-moduli:

$$\hat{\Gamma}_{m,n}(\nu = \ell\nu_0) = \sum_k g_{X_m}(\ell,k)g_{X_n}^*(\ell,k) \tag{1}$$

Straightforward calculations yield

$$\mathbb{E}\hat{\Gamma}_{m,n}(\nu = \ell\nu_0) = \int \Gamma_{m,n}(f - \ell\nu_0)|\tilde{\phi}(f)|^2\,df \tag{2}$$

thus showing that $\hat{\Gamma}_{m,n}(\nu)$ estimates $\Gamma_{m,n}(\nu)$ by averaging $\Gamma_{m,n}(f)$ over frequencies f within a spectral band controlled by $\tilde{\phi}$. The time and frequency resolutions of the functions $\phi_{\ell,k}$ depend neither on ℓ nor on k, and are only controlled through the choice of the function ϕ. STFT thus achieves a fixed *absolute-frequency resolution* multivariate spectral analysis.

Of particular interest in multivariate analysis is the pairwise coherence function

$$\mathrm{Coh}_{m,n}(f) = \frac{\Gamma_{m,n}(f)}{\sqrt{\Gamma_{m,m}(f)\Gamma_{n,n}(f)}} \tag{3}$$

which consists of a frequency-dependent correlation coefficient. By quantifying which frequencies are actually involved in cross-temporal dynamics, it permits better analysis of the overall temporal dynamics of a system. For real signals, $C_{m,n}(f)$ is also real and ranges within $-1 \leq \mathrm{Coh}_{m,n}(f) \leq 1$.

2.2. Wavelet-based spectral estimation

2.2.1. Multivariate wavelet transform

As an alternative to the STFT, spectral estimation can be reformulated using the discrete wavelet transform (DWT). The coefficients of the DWT, $d_X(j,k)$, are defined by comparing, by means of inner products, the signal to analyze, $X(t)$, against a collection of translated and dilated templates, $\psi_{j,k}(t) = 1/a_0^j\psi((t - kT_0a_0^j)/a_0^j)$, of a finite-energy reference pattern $\psi(t)$: $d_X(j,k) = \langle X, \psi_{j,k}\rangle$. When ψ is a zero-mean function, $\int \psi(t)\,dt \equiv 0$, and under other mild conditions, the time and scale resolutions T_0 and a_0 can be chosen such that the DWT can be inverted and the $d_X(j,k)$ can be interpreted as the joint time and scale content of X around time $t = ka_0^jT_0$ and scale $a = a_0^j$. Additionally, for appropriate ψ, the set $\{a_0^{j/2}\psi_{j,k}(t)\}_{j,k\in\mathbb{R}^2}$ is an orthonormal basis of $L^2(\mathbb{R})$, thus leading to simple inversion algorithms. The generic case of the dyadic DWT, used here, corresponds to selecting $a_0 = 2$ [36,37].

In addition to being band-pass, the mother wavelet ψ is often designed to have N_ψ vanishing moments, with N_ψ defined as the smallest integer such that

$$\forall k = 0\ldots,N_\psi - 1, \quad \int t^k\psi(t)\,dt \equiv 0 \quad \text{and} \quad \int t^{N_\psi}\psi(t)\,dt \neq 0 \tag{4}$$

N_ψ controls the decay of $\tilde{\psi}$ around $\nu = 0$ as: $|\tilde{\psi}(\nu)| \simeq C_\psi|\nu|^{N_\psi}$, and thus the bandwidth of $\tilde{\psi}$ [36,37].

The band-pass nature of ψ permits the association with characteristic central frequency ν_ψ and bandwidth $\Delta\nu_\psi$:

$$\nu_\psi = \frac{\int f|\tilde{\psi}(f)|^2\,df}{\int |\tilde{\psi}(f)|^2\,df} \quad \text{and} \quad \Delta\nu_\psi = \sqrt{\frac{\int |f - \nu_\psi|^2|\tilde{\psi}(f)|^2\,df}{\int |\tilde{\psi}(f)|^2\,df}} \tag{5}$$

Thus, by remapping the scale a to the frequency ν via $\nu = \nu_\psi/a$, the DWT coefficients $d_X(j,k)$ can also be interpreted as the joint time and frequency content of X around time $t = ka_0^jT_0$ and frequency $\nu = \nu_\psi/a_0^j$ [8,40].

2.2.2. Multivariate wavelet-based spectral estimation

DWT-based multivariate spectral analysis amounts to estimating $\Gamma_{m,n}(\nu)$ by time averages of DWT coefficients squared-moduli:

$$\hat{\Gamma}_{m,n}^{(W)}(\nu = \nu_\psi/a_0^j) = \sum_k d_{X_m}(j,k)d_{X_n}^*(j,k) \tag{6}$$

Straightforward calculations yield:

$$\mathbb{E}\hat{\Gamma}_{m,n}^{(W)}(\nu = \nu_\psi/a_0^j) = \int \Gamma_{m,n}(f)|\tilde{\psi}(f/a_0^j)|^2 \, \mathrm{d}f \tag{7}$$

The central frequency, the time, and the frequency resolution of $\psi_{j,k}$ are related to those of ψ as $\nu_{j,k} = \nu_\psi/a_0^j$, $\Delta\nu_{j,k} = \Delta\nu_\psi/a_0^j$ and $\Delta T_{j,k} = \Delta T_\psi \times a_0^j$. This shows that $\hat{\Gamma}_{m,n}^{(W)}(\nu)$ estimates $\Gamma_{m,n}(\nu_\psi/a_0^j)$ by averaging $\Gamma_{m,n}$ over frequencies f around ν_ψ/a_0^j within a spectral band controlled by $\Delta\nu_\psi/a_0^j$. DWT thus achieves a *fixed relative-frequency* resolution multivariate spectral analysis.

In analogy to the coherence function, the wavelet coherence can be defined as [48]:

$$\mathrm{Coh}_{m,n}^{(W)}(\nu = \nu_\psi/a) = \frac{\Gamma_{m,n}^{(W)}(\nu_\psi/a)}{\sqrt{\Gamma_{m,m}^{(W)}(\nu_\psi/a)\Gamma_{n,n}^{(W)}(\nu_\psi/a)}} \tag{8}$$

For real signals, it ranges within $-1 \leq \mathrm{Coh}_{m,n}^{(W)} \leq 1$ and quantifies, as a scale-dependent correlation coefficient, which scales are actually involved in cross-temporal dynamics, and thus permits to better analyze the overall temporal dynamics of a scale-free system.

2.3. Fourier vs. wavelet: oscillatory vs. scale-free dynamics

Theoretically, STFT and DWT lead to valid representations of X that do not lose information. This is so because they can be inverted, i.e. X can be exactly recovered from the representation coefficients $g_X(\ell,k)$ or $d_X(j,k)$. Thus, both versions of spectral estimation provide alternative and consistent estimators of $\Gamma_{m,n}(\nu)$: $\hat{\Gamma}_{m,n}(\nu = l\nu_0)$ and $\hat{\Gamma}_{m,n}^{(W)}(\nu = \nu_\psi/a_0^j)$.

The *equivalence* between both estimation methods is illustrated empirically in Fig. 1. Based on several examples of bivariate time series, the figure shows that the plot of $\log_2 \hat{\Gamma}_{m,n}(\nu)$ as a function of $\log_2 \nu = \ell\nu_0$ superimposes well on the plot of $\log_2 \hat{\Gamma}_{m,n}^{(W)}(\nu)$ as a function of $\log_2 \nu = \nu_\psi/a$, when $\nu_\psi/a = \ell\nu_0$.

Thus, both spectral estimation methods can be of interest, depending on the temporal dynamics of the data. When temporal dynamics are better characterized by oscillatory behaviors, STFT-based spectral estimation provides accurate estimation of energies in the corresponding frequency band, while DWT-based spectral estimation is better suited for the analysis of scale-free dynamics. This is illustrated in Fig. 1 (top row), showing superimposed spectral estimates for synthetic signals consisting of (additive) mixtures of oscillatory and scale-free dynamics. Spectral-based estimates better locate the frequency of the oscillatory modes, and better quantify the low coherence level at corresponding frequencies. By contrast, wavelet-based estimates better reveal power-law behavior down to lower frequencies. This permits better estimation of the scaling exponents and, hence, more accurate analysis of the scale-free dynamics.

2.4. Wavelets and scale-free dynamics

Historically, scale-free dynamics has been modeled by stationary processes with Fourier spectra satisfying an asymptotic power law (hence, scale-free) behavior in the low-frequency limit: $\forall m,n, \Gamma_{m,n}(\nu) \simeq \gamma_{m,n}|\nu|^{\beta_{m,n}}$ for $\nu \to 0$. For such processes, a simple change of variable in Eq. (7) above, permitted by the dilation operator underlying the definition of the DWT, shows that the DWT-based spectral analysis accurately reproduces asymptotic power-law behavior in the coarse scale limit, i.e. when $j \to +\infty$:

$$\mathbb{E}\hat{\Gamma}_{m,n}^{(W)}(\nu = \nu_\psi/a_0^j) = \gamma_{m,n}^{(W)} a_0^{2j\beta_{m,n}} \text{ with } \gamma_{m,n}^{(W)} = \left(\gamma_{m,n}\int |f|^{\beta_{m,n}}|\tilde{\psi}(f)|^2 \, \mathrm{d}f\right) \tag{9}$$

The frequency-shift operator underlying the STFT does not permit such a change of variable, which leads to significantly biased estimates of power-law behavior. Less accurate estimation of the scaling exponents $\beta_{m,n}$ follows, in turn yielding poorer analysis of temporal (scale-free) dynamics [8,10,38–41]. This is illustrated in Fig. 1 (second row) with multivariate fractional Gaussian noise, used as a cornerstone model for scale-free dynamics, and defined as the increment process of multivariate fractional Brownian motion (see Section 3 for a definition). Wavelet-based spectral estimates perfectly reveal the power-law behaviors down to low frequencies and a constant level of the wavelet coherence function across all frequencies, thus permitting a relevant characterization of multivariate scale-free dynamics.
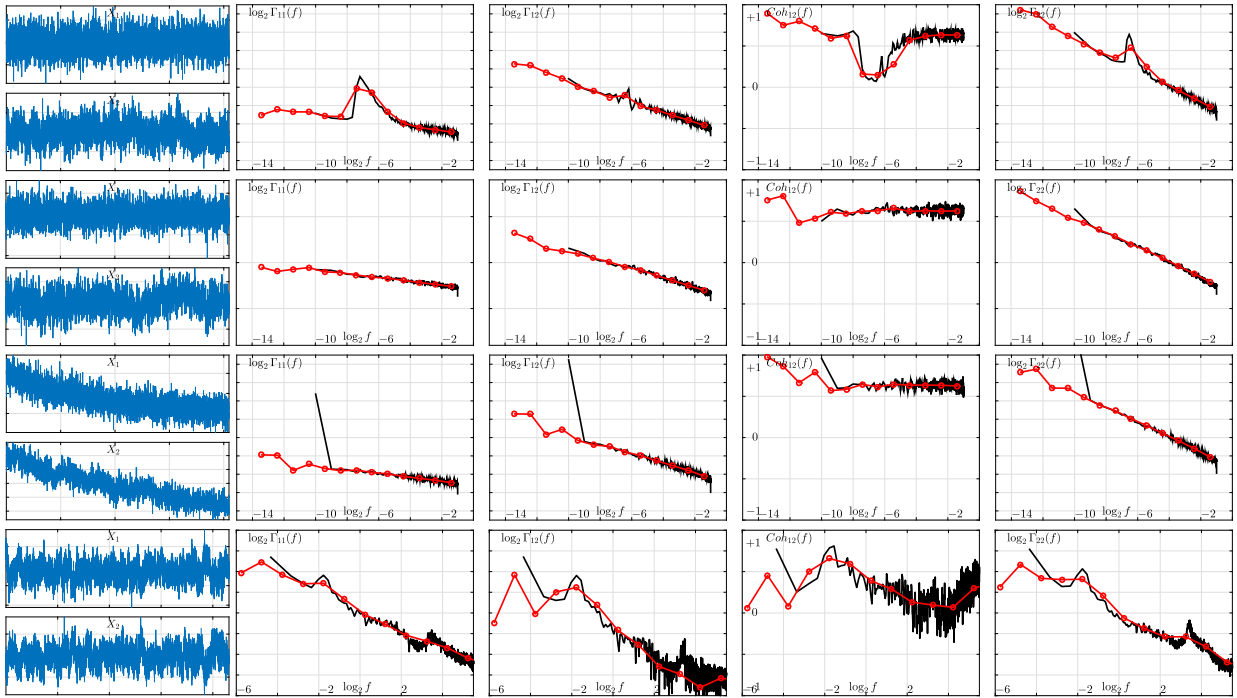
(a) Time series. (b) Spectra for each component (left, right), Cross-spectra (center left), Coherences (center right).

Fig. 1. Fourier versus wavelet spectral estimation. Superimposed Fourier (black lines) and wavelet spectra (red dotted lines) for synthetic signals with additive mixture of scale-free and oscillatory dynamics (top row), with scale-free dynamics (second row), with scale-free dynamics and smooth slowly decaying (exponential) additive trends (third row), and for MEG data (bottom row).

2.5. Wavelet-based spectral estimation and robustness to trends

Besides being better-suited to the analysis of scale-free temporal dynamics, DWT-based spectral estimation benefits from further practical robustness. This is notably the case when smooth trends are superimposed on the data under scrutiny. This is illustrated qualitatively in Fig. 1 (third row) where unrelated deterministic smooth (e.g., algebraic or exponential) trends are added to each component of a bivariate fractional Gaussian noise. Fourier-based spectral analysis is clearly strongly biased at low frequencies by the smooth trends, and so is the coherence function. By contrast, wavelet-based spectral analysis perfectly reveals the multivariate scale-free temporal dynamics across all frequencies, as well as the constant level of the coherence across scales, in perfect match with the multivariate fractional Gaussian noise models used here [41,49].

2.6. Macroscopic infraslow brain activity, scale-free dynamics and wavelet-based spectral estimation

Fig. 1 (fourth row) further compares Fourier-based and wavelet-based spectral estimations for a pair of MEG time series recorded on a subject at rest.[1] These spectral estimates show that brain macroscopic activity consists of a mixture of both oscillatory behaviors in well-established frequency bands, each associated with specific brain functions, and infraslow scale-free dynamics. The alpha-band, $8 \leq f \leq 12$ Hz, corresponding to attention, displays significant power in this range, that can be well analyzed and quantified using Fourier-based spectral estimation. In addition, the infraslow ($f \leq 3$ Hz) brain dynamics is characterized by the absence of characteristic oscillations, hence by scale-free dynamics. Initially thought to be experimental noise or head-movement induced, this infraslow activity has now been recognized to be associated with the range of frequencies where most brain energy is consumed and is now viewed as the signature of spontaneous brain activity. Notably, it has been consistently shown that the brain at rest shows strong infraslow scale-free dynamics that structures functional connectivity (e.g., with the resting state network) [23,24]. It is now commonly considered that the modifications induced by task engagement in brain activity can be quantified by departure from resting state activity, in particular with a region-dependent decrease of the scaling exponents quantifying the scale-free dynamics (hence, of the overall temporal correlations) [24,26,35].

---

[1] Data courtesy NeuroSpin, Ph. Ciuciu and V. van Wassenhove [50].

3. Wavelet eigenanalysis of multivariate self-similarity

3.1. Multivariate self-similarity

Following the seminal intuitions of B. Mandelbrot [51], scale-free dynamics has often been modeled as self-similarity [52]. The celebrated fractional Brownian motion (fBm), $B_H(t)$, is defined as the only Gaussian self-similar process with stationary increments. Together with its increment process, called fractional Gaussian noise (fGn), it has been massively used in the modeling of scale-free temporal dynamics for univariate data. For univariate stochastic processes, self-similarity is defined as scale invariance of all finite-dimensional distributions under dilation, i.e., for any dilation factor $a > 0$,

$$\{B_H(t)\}_{t\in\mathbb{R}} \stackrel{\text{fdd}}{=} \{a^H B_H(t/a)\}_{t\in\mathbb{R}} \tag{10}$$

where H is the *self-similarity parameter*, or *scaling exponent* and where $\stackrel{\text{fdd}}{=}$ denotes equality for all finite dimensional distributions. The assumptions of stationary increments and finite variance confine H inside the interval $(0, 1]$.

Though seemingly intuitive, a canonical model for multivariate self-similarity called Operator fractional Brownian motion (OfBm) was only recently defined [42,53–55]. OfBm arises as a weak limit of multivariate time series displaying matrix-induced memory properties [56,57]. It also provides a natural framework for the modeling of Internet traffic [44], dendrochronology [58] and fractional cointegration [59]. Hereinafter, use is made of a less general yet more pedagogical and constructive definition, which also constitutes a special yet broad subclass of OfBm, referred to here as multivariate fBm (MfBm).

First, let $B_{\underline{H},\Sigma}(t)$ be a collection of M fBm $B_{H_m}(t)$, each with a potentially different self-similarity exponent H_m. These M-components are pointwise correlated according to a $M \times M$ symmetric positive definite (covariance) matrix Σ. Second, let W denote a $M \times M$ invertible matrix. Then, MfBm, $B_{\underline{H},\Sigma,W}(t)$ is defined by a linear mixing of $B_{\underline{H},\Sigma}(t)$ according to W:

$$B_{\underline{H},\Sigma,W}(t) = W B_{\underline{H},\Sigma}(t) \tag{11}$$

Hence, MfBm is parametrized by the vector of scaling exponents $\underline{H} = (H_1 \ldots, H_m)$, the mixing matrix W, and the covariance matrix Σ.

Multivariate self-similarity translates into the finite-dimensional equality of the joint or multivariate finite-dimensional distributions:

$$\forall a > 0, \qquad \{B_{\underline{H},\Sigma,W}(t)\}_{t\in\mathbb{R}} \stackrel{\text{fdd}}{=} \{a^{\underline{H}} B_{\underline{H},\Sigma,W}(t/a)\}_{t\in\mathbb{R}} \tag{12}$$

with $a^{\underline{H}} := \sum_{k=0}^{+\infty} \log^k(a)\underline{H}^k/k!$ and where $\underline{H} = W\,\text{diag}\underline{H}W^{-1}$ is now an $M \times M$ matrix of scaling exponents.

3.2. Wavelet analysis of multivariate self-similarity

3.2.1. Multivariate wavelet eigenanalysis
Extending spectral analysis to a multivariate setting and applying wavelet analysis to MfBm lead to a scale-dependent collection of $M \times M$ (wavelet) matrices $S(j)$ with entries

$$S_{m,n}(j) = 1/n_j \sum_k d_{(B_{\underline{H},\Sigma,W})_m}(j,k)d_{(B_{\underline{H},\Sigma,W})_n}(j,k) \tag{13}$$

While the classical analysis of multivariate self-similarity would consist of analyzing each entry $S_{m,n}(j)$ independently as a function of scales $a = 2^j$ and possibly estimating the corresponding scaling exponent, an original wavelet eigenanalysis approach was recently proposed [43,44]. The approach reverses the perspective on multivariate multiscale analysis: it first considers the full matrix S at a given scale $a = 2^j$ by computing the eigenvalues $\Lambda_1(j)\ldots, \Lambda_M(j)$, and, second, it takes advantage of the behavior of each $\Lambda_m(j)$ as a function of scales 2^j by possibly estimating the corresponding scaling exponents.

Notably, for MfBm, it has been shown that, in the asymptotic limit of coarse scales, the eigenfunctions $\Lambda_m(j)$ reproduce multivariate self-similarity as [43,44]:

$$\Lambda_m(j) \simeq \lambda_m 2^{2jH_m}, \ 2^j \to +\infty \tag{14}$$

with λ_m depending on Σ, W and ψ.

3.2.2. Non-mixed multivariate self-similarity
To develop more intuition into the potential of the wavelet eigenanalysis, let us first study the simpler case where there is no mixing, i.e. the mixing matrix reduces to the identity matrix $W \equiv I_M$. Multivariate self-similarity then simplifies to M univariate self-similarity relations, i.e.
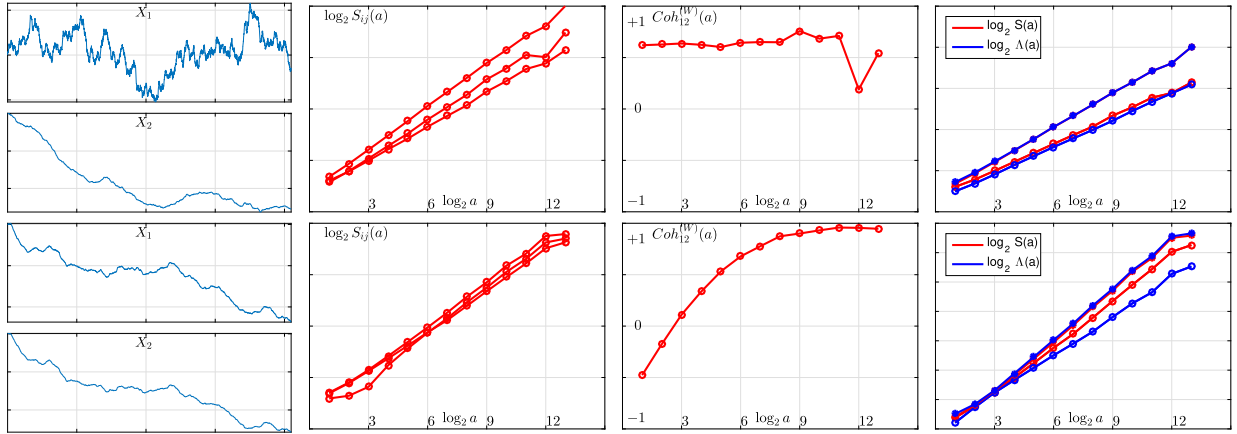
(a) Time series

(b) Bivariate wavelet analysis. $\log_2 S_{11}(a)$, $\log_2 S_{12}(a)$ and $\log_2 S_{22}(a)$ as functions of $\log_2 a$ (left) ; wavelet coherence function (center); wavelet eigenfunctions $\log_2 \Lambda_1(a)$ and $\log_2 \Lambda_2(a)$ compared to wavelet univariate spectra $\log_2 S_{11}(a)$ and $\log_2 S_{22}(a)$ (right).

Fig. 2. Multivariate self-similarity. Non-mixed OfBm (top row), and mixed OfBm (bottom row). Wavelet (cross)-spectra (center left), wavelet coherence function (center left), wavelet eigenanalysis compared to wavelet spectra (right).

$$\{B_{H_1}(t), \ldots, B_{H_M}(t)\}_{t\in\mathbb{R}} \overset{\text{fdd}}{=} \{a^{H_1} B_{H_1}(t/a), \ldots, a^{H_M} B_{H_M}(t/a)\}_{t\in\mathbb{R}} \tag{15}$$

Hence, the entrywise covariance functions of MfBm reduce to

$$\mathbb{E} B_{H_m}(t) B_{H_n}(s) = \Sigma_{m,n}(|t|^{H_m+H_n} + |s|^{H_m+H_n} - |t-s|^{H_m+H_n}) \tag{16}$$

By combining the definition of DWT and the covariance of non-mixed MfBm, one can show that

$$\forall m, n, \quad \forall j > 0, \qquad \mathbb{E} S_{m,n}(j) = w_{\underline{H}, \Sigma, \psi} 2^{j(H_m+H_n)} \tag{17}$$

with parameters $w_{\underline{H}, \Sigma, \psi}$ depending jointly on $\underline{H}$, Σ and ψ. Calculations and proofs closely follow the wavelet analysis of univariate self-similarity [43,44].

These power-law behaviors are illustrated with bivariate MfBm in Fig. 2 (top row, center left). They call for the following comments.

First, because it is constructed from a dilation operator, wavelet analysis exactly reproduces self-similarity (while Fourier analysis would not, cf. [40] for a more complete and richer discussion). Hence, this leads to efficient estimation of the scaling exponents $H_m + H_n$ (cf., e.g., [8]). Intuitively, this can be interpreted as the fact that wavelet analysis extends spectral analysis to multivariate nonstationary processes, yet with stationary increments. This can be generalized to processes with stationary higher-order increments (increments of increments...), provided that the number of vanishing moments of the mother-wavelet N_ψ is increased accordingly.

Second, for non-mixed MfBm, multivariate (or eigen) wavelet analysis is redundant. There are $M \times M$ potentially usable entries in the matrix S, whereas multivariate self-similarity analysis reduces to estimating only M scaling exponents. This is illustrated by the facts that i) the wavelet coherence function is constant across the scales $a = 2^j$ actually measuring the overall correlation coefficients (Fig. 2 top row, center left); and that ii) the eigenfunctions $\Lambda_1(j)$ and $\Lambda_2(j)$ reproduce the power-law behavior of the wavelet autospectra $S_{11}(j)$ and $S_{22}(j)$, with the same scaling exponents $2H_1$ and $2H_2$ (Fig. 2 top row, left). This can be used to robustify the estimation of scaling exponents [60], to test the absence of mixing, or to assess departures from non-mixed multivariate self-similarity (also referred to as fractal connectivity) [49]. In particular, this has been used to enrich the quantification and assessment of functional connectivity in neuroscience [35,61].

3.2.3. Mixed multivariate self-similarity

To further gain intuition into the potential of wavelet eigenanalysis, let us now consider mixed MfBm, i.e. with a mixing matrix W that is unknown and not necessarily diagonal. In that case, multivariate self-similarity becomes far more intricate to analyze. Indeed, the covariance of mixed MfBm $B_{\underline{H}, \Sigma, W}$

$$\Sigma_{B_{\underline{H}, \Sigma, W}} = W \Sigma_{B_{\underline{H}, \Sigma}} W^\top \tag{18}$$

mixes together additively power laws, with different scaling exponents involving pair-combinations from the entire vector $\underline{H}$ [43,44]. Computing the collection of $M \times M$ matrices $S(j)$ from mixed MfBm results in the same intricate situation, $\forall m, n, \forall j > 0$, $\mathbb{E} S_{m,n}(j)$, consists of additive mixtures of $M(M+1)/2$ power laws, combining all possible pairs of exponents $H_k + H_l$, and the coefficients of the mixtures depend simultaneously on $\underline{H}$, Σ and W [43,44,62]. This is illustrated in Fig. 2

(bottom row, center left) for bivariate MfBm, where the functions $\log_2 S_{11}(j)$, $\log_2 S_{12}(j)$ and $\log_2 S_{22}(j)$ as functions of the log-scales $\log_2 a$ tend to superimpose. Classical wavelet analysis leads to the conclusion that a single exponent (i.e. the largest) drives the temporal dynamics of data. The estimation of scaling exponents by solving the non-convex optimization problem of fitting additive mixtures of power laws, though doable in principle, turns out to be not feasible in practice beyond the bivariate case $M = 2$ [62]. However, the wavelet coherence function, being non-constant across scales, already provides an indication that data may not be driven by a single scaling exponent (Fig. 2, bottom row, center right).

The wavelet-eigenanalysis approach actually permits the disentangling of mixed multivariate self-similarity. Indeed, the function $\log_2 \Lambda_2(j)$ shows the same (dominant) scaling behavior as the one observed in $\log_2 S_{11}(j)$, $\log_2 S_{12}(j)$, and $\log_2 S_{22}(j)$. However, the evolution of $\log_2 \Lambda_1(j)$ as a function of scales departs from the dominant behavior. It actually reveals the non-dominant scaling exponent, which is hidden by force of mixing, but is still present in the joint structure of data. Multivariate wavelet analysis thus permits the accurate disentangled analysis of multivariate self-similarity and efficient estimation of the M scaling exponents [43,44] by operating a change of perspective: The independent univariate analysis of the M-components of multivariate MfBm first inspects the temporal dynamics of each component across scales and then compares components ones against the others, resulting in possibly strongly inaccurate analysis. By contrast, multivariate wavelet eigenanalysis first investigates all components jointly at a given scale 2^j (by computing an eigenvalue decomposition), and then uses the behavior of the eigenvalues across scales as an analysis tool.

Estimating the mixing matrix is generally doable only in the context of independent sources (when Σ is diagonal). This is a different topic, and it is not addressed here; interested readers are referred to [58].

4. Multivariate multifractality

4.1. Beyond second-order analysis: multifractal analysis

It can happen that data have exactly the same marginal distributions (one-point statistics) and the same covariance functions or Fourier spectrum (2-point statistics), but are different. Distinguishing between such data requires analysis tools designed to go beyond covariance analysis. In the context of scale-free temporal dynamics characterization, multifractal analysis provides such a tool.

In essence, multifractal analysis aims to characterize the fluctuations along time of local regularity in a signal $X(t)$, cf., e.g., [63–65]. Local regularity can be quantified by pointwise exponents, the most common one being the Hölder exponent, $h(t) \geq 0$, defined as follows: X belongs to $C^\alpha(t)$, $\alpha \geq 0$, if there exist a polynomial P_t with $\deg(P_t) < \alpha$ and a constant $C > 0$ such that: $|X(t + a) - P_t(t + a)| \leq C|a|^\alpha$ when $|a| \to 0$. The Hölder exponent consists of the largest such α: $h(t) \triangleq \sup\{\alpha : X \in C^\alpha(t)\} \geq 0$. Essentially, the larger $h(t)$, the smoother X around t, and conversely, the closer $h(t)$ to 0, the more irregular X at t. Other exponents, such as p-exponents, generalize the use of Hölder exponents [66,67]. Hereafter, we use generically $h(t)$ to denote either Hölder exponent or p-exponents.

Some processes display smooth regularity exponents. This is the case for MfBm: $h(t)$ is constant for each component. However, in general, $h(t)$ is so irregular that one cannot base the analysis on the time evolutions of the functions $h_1(t)\ldots, h_M(t)$ obtained independently from each component of multivariate data. Instead, multifractal analysis aims to provide a global, geometric, and multivariate description of the temporal dynamics of X via the so-called multivariate multifractal spectrum $D(h_1\ldots, h_M)$, defined as the collection of Hausdorff dimensions $\dim_H$ of the sets of points $t \in \mathbb{R}$ where $(h_1(t)\ldots, h_M(t))$ takes the same values $\underline{h} \equiv (h_1\ldots, h_M)$ [46]:

$$\mathcal{D}(\underline{h}) \triangleq \dim_H \left\{ t : (h_1(t)\ldots, h_M(t)) = \underline{h} \right\} \tag{19}$$

The multifractal spectrum $\mathcal{D}(\underline{h})$ can thus be considered as an efficient summary of the multivariate temporal dynamics of data X.

4.2. Multifractal formalism

Standard multifractal models lead to highly irregular exponents $h_m(t)$ that cannot be estimated in practice [63–65] and the numerical estimation procedure for $\mathcal{D}(\underline{h})$ from data, referred to as the *multifractal formalism*, requires the use of new *multiscale quantities*, beyond wavelet coefficients, which match the pointwise exponent chosen to quantify regularity.

It is now well documented [65–67] that measuring Hölder exponents (or p-exponents) calls for the use of *wavelet leaders* (or *p-leaders*). These are defined as local l^∞ or l^p-norms of wavelet coefficients:

$$\ell_X(j, k) \triangleq \sup_{2^{j'} k' \in 3\lambda_{j,k}} \left| d_X(j', k') \right| \quad \text{or} \quad \ell_X^{(p)}(j, k) \triangleq \left(\sum_{2^{j'} k' \in 3\lambda_{j,k}} \left| d_X(j', k') \right|^p 2^{(j-j')} \right)^{1/p} \tag{20}$$

where $\lambda_{j,k} = [k2^j, (k+1)2^j)$ is a dyadic interval of size 2^j and $3\lambda_{j,k} \triangleq \lambda_{j,k-1} \cup \lambda_{j,k} \cup \lambda_{j,k+1}$ is the union of $\lambda_{j,k}$ with its two neighbors.

Following spectral estimation and extending to higher statistical orders and to p-leaders the wavelet spectrum $S(j)$, one can form a collection of multiscale functions $L_{\underline{q}}(j)$ parametrized with $\underline{q} = (q_1, \ldots, q_M)$, defined as

$$L_{\underline{q}}(j) = \frac{1}{n_j} \sum_{k=1}^{n_j} \ell_{X_1}^{(p)}(j,k)^{q_1} \times \ldots \times \ell_{X_M}^{(p)}(j,k)^{q_M} \tag{21}$$

For numerous classes of processes with scale-free dynamics, it is experimentally observed that, in the limit of fine scales,

$$L_{\underline{q}}(j) \sim K_{q_1 \ldots q_M} 2^{j\zeta(\underline{q})}, \ 2^j \to 0 \tag{22}$$

The *scaling exponents* $\zeta(\underline{q})$ can thus be estimated by linear regression [65,67].

The multivariate Legendre transform can be derived from $\zeta(\underline{q})$ through a multivariate Legendre transform

$$\mathcal{L}(\underline{h}) = \inf_{\underline{q}}(1 + \langle \underline{q}, \underline{h} \rangle - \zeta(\underline{h})) \tag{23}$$

4.3. Limitations

In the univariate setting, $M = 1$, the Legendre spectrum always provides an upper-bound estimate of the multifractal spectrum, $\mathcal{L}(h) \geq \mathcal{D}(h)$, where the inequality turns into an equality for large classes of processes [64].

In the multivariate setting, it was recently shown that the multivariate Legendre spectrum does not always yield an upper-bound estimate of the multivariate multifractal spectrum, see [46,68] for a detailed analysis of this intricate issue. However, it is expected that the inequality (and even the equality) holds for large classes of processes, and that it can be useful for real-world data modeling. Some theoretical guidelines are provided in [68]; additionally, generic results of validity are proved in [69].

4.4. Multifractal formalism in practice

Even though the Legendre spectrum does not necessarily estimate the multifractal spectrum, the scaling exponents $\zeta(\underline{q})$ convey information of any statistical order related to temporal dynamics and are thus of interest in characterizing scale-free dynamics. However, because estimating a multivariate function is difficult, we propose a polynomial expansion that generalizes to the multivariate setting the strategy proposed in [70,71] for the univariate case. For ease of exposition, the discussion here is restricted to a bivariate setting, $M = 2$. The scaling exponents can thus be approximated as $\zeta(q_1, q_2) = c_{10}q_1 + c_{01}q_2 + c_{20}q_1^2 + c_{02}q_2^2 + c_{11}q_1q_2 + \ldots$

Under mild conditions, it can be shown that the coefficients $c_{n_1n_2}$ (with $n_1 + n_2 = n$) entering the expansion can be related to the multivariate cumulants of order n, $C_{n_1n_2}(j)$, of the multivariate variables $\{\log \ell_{X_1}^{(p)}(j,k) \ldots, \log \ell_{X_M}^{(p)}(j,k)\}$. Indeed, for certain classes of multivariate multifractal processes [68], it is observed that

$$C_{n_1n_2}(j) = c_{n_1n_2}^0 + c_{n_1n_2} \log 2^j \tag{24}$$

The first-order cumulants ($n = 1$, $C_{10}(j)$ and $C_{01}(j)$) convey information mostly driven by the covariance function of the process X and, hence, are closely related to the functions $\log_2 S_{10}(j)$ and $\log_2 S_{01}(j)$ [72,73].

The higher-order cumulants ($n \geq 2$, $C_{20}(j)$, $C_{02}(j)$, $C_{11}(j) \ldots$) convey information on temporal dynamics beyond second-order statistics, which is not already encoded in the covariance functions.

This materializes through an approximation of the bivariate Legendre spectrum as:

$$\mathcal{L}(h_1, h_2) \approx 1 + \frac{c_{02}b}{2}\left(\frac{h_1 - c_{10}}{b}\right)^2 + \frac{c_{20}b}{2}\left(\frac{h_2 - c_{01}}{b}\right)^2 - c_{11}b\left(\frac{h_1 - c_{10}}{b}\right)\left(\frac{h_2 - c_{01}}{b}\right) \tag{25}$$

where $b \triangleq c_{20}c_{02} - c_{11}^2 \geq 0$, thus showing that the position of the maximum of the bivariate spectrum is given by $\mathbf{h}^m = (c_{10}, c_{01})$ and, further, that the coefficients c_{20}, c_{02}, and c_{11} characterize the multifractal properties of X, notably with c_{11} encoding cross-multifractality.

Furthermore, by taking inspiration from the wavelet coherence function (see Eq. (3)), we propose to define a wavelet leader multifractal coherence function as:

$$\text{Coh}^{(\text{mf})}(j) = \frac{C_{11}(j)}{\sqrt{C_{20}(j) \times C_{02}(j)}} \tag{26}$$

On a scale-by-scale basis, this quantifies cross-dependencies amongst the components of the data that are not already accounted for by the wavelet coherence function.

Fig. 3 illustrates the theory and practice of multifractal analysis based on several different synthetic processes and MEG data. Use is made of the bivariate multifractal random walk (bi-MRW), a cornerstone multifractal process, designed here
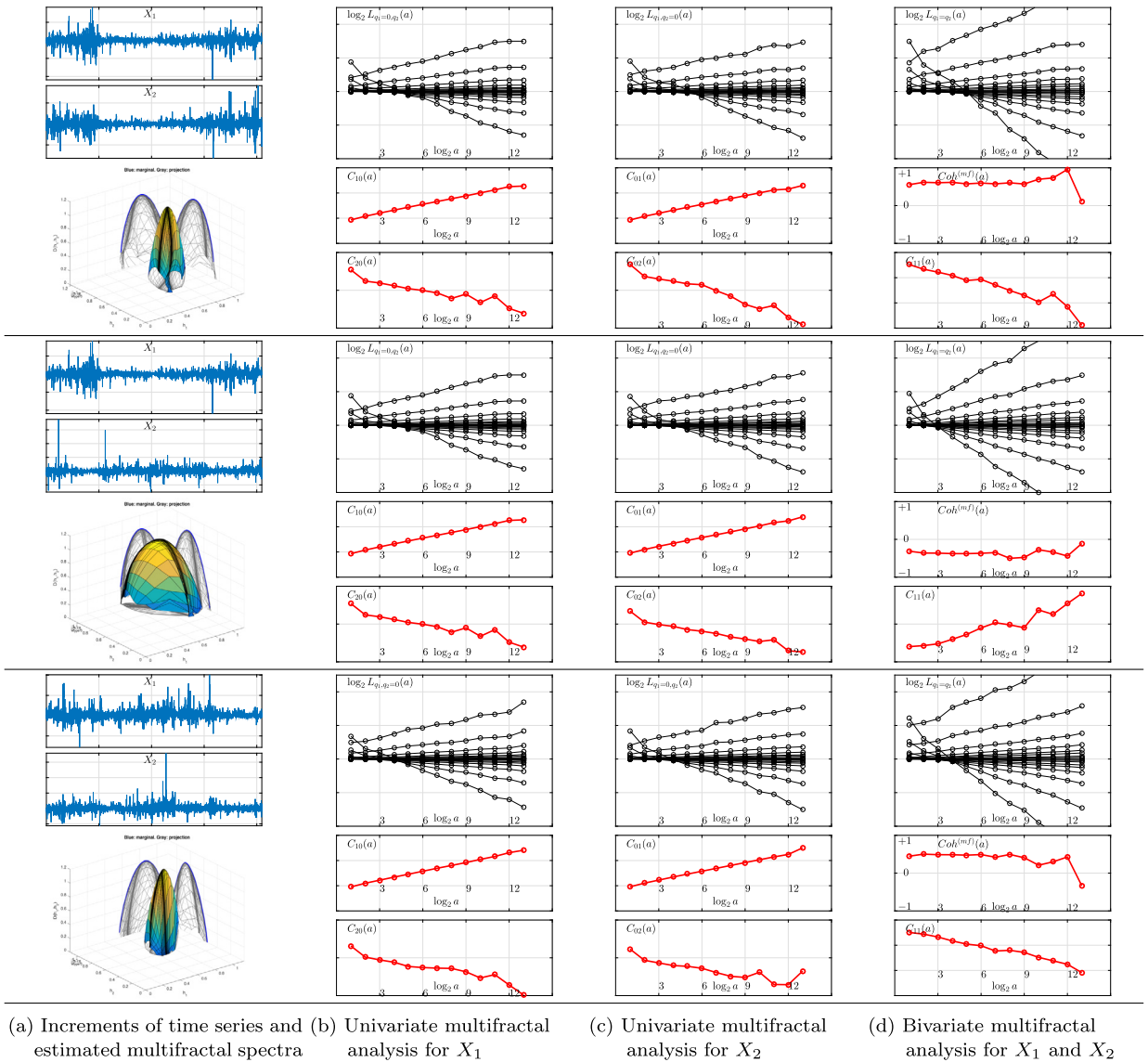
(a) Increments of time series and estimated multifractal spectra

(b) Univariate multifractal analysis for X_1

(c) Univariate multifractal analysis for X_2

(d) Bivariate multifractal analysis for X_1 and X_2

Fig. 3. Empirical bivariate multifractal analysis. From top to bottom: correlated bivariate MRW, anticorrelated bivariate MRW, uncorrelated bivariate MRW. From left to right: increments of the time series and univariate and bivariate multifractal spectra; univariate analysis for component 1 with $\log_2 L_{0,q}(j)$, $C_{10}(j)$ and $C_{20}(j)$ as functions of $\log_2 a$ univariate analysis for component 2 with $\log_2 L_{q,0}(j)$, $C_{01}(j)$ and $C_{02}(j)$ as functions of $\log_2 a$; bivariate analysis for components 1 and 2 with $\log_2 L_{q_1,q_2}(j)$, $\text{Coh}^{(\text{mf})}(j)$ and $C_{11}(j)$ as functions of $\log_2 a$.

as an extension of the univariate MRW construction in [74] by combining bivariate OfBm synthesis [75] with bivariate multifractal construction [72,73].

Fig. 3 (top pair of rows) shows the increments of a correlated bi-MRW and the (wavelet p-leader-based) estimates of univariate and bivariate multifractal spectra (right), the univariate multifractal analysis of component 1 and component 2 (center right and left), and the bivariate multifractal analysis of components 1 and 2 with the leader-based multifractal coherence function (left). The multifractality of each component as well as cross-multifractality are assessed by means of the linear behavior of the functions $\log_2 L_{q,0}(j)$, $\log_2 L_{0,q}(j)$ and $\log_2 L_{q_1,q_2}(j)$ with respect to the log-scales $\log_2 a = j$, or equivalently, by the linear behavior of functions $C_{10}(j)$, $C_{01}(j)$, $C_{20}(j)$, $C_{02}(j)$, and $C_{11}(j)$. The estimated Legendre spectrum $\mathcal{L}(h_1, h_2)$ departs from the simple form $\mathcal{L}_1(h_1) + \mathcal{L}_2(h_2) - 1$ (which is expected for independent processes); this constitutes a strong indication of the presence of statistical dependencies not already quantified by the coherence functions. Such dependencies are further quantified by the wavelet leader multifractal coherence function $\text{Coh}^{(\text{mf})}(j)$, which shows a positive constant behavior across scales. This indicates temporal coincidences of the largest or smallest regularity exponents within the two components.
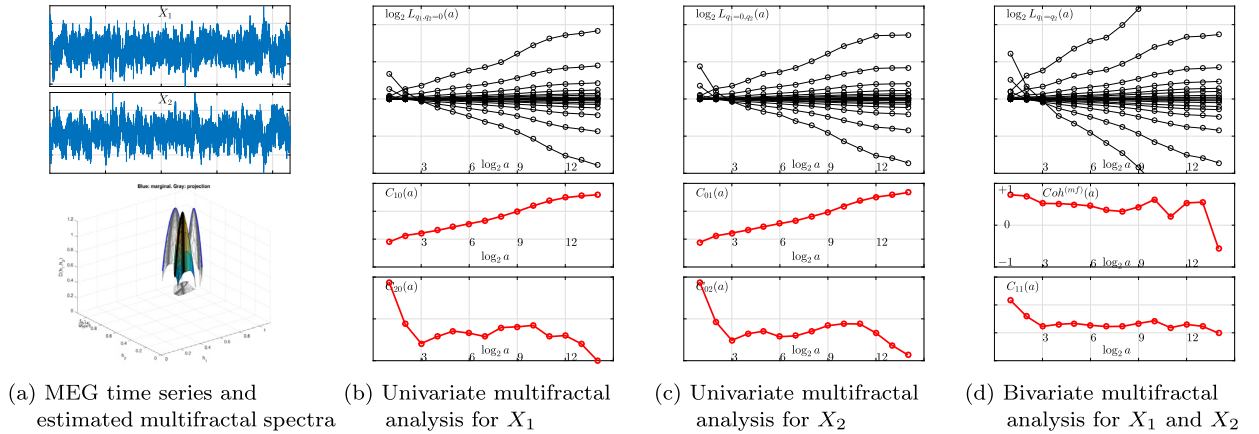
(a) MEG time series and estimated multifractal spectra

(b) Univariate multifractal analysis for X_1

(c) Univariate multifractal analysis for X_2

(d) Bivariate multifractal analysis for X_1 and X_2

Fig. 4. MEG Data bivariate multifractal analysis. Macroscopic brain activity MEG data. From left to right: increments of the time series and univariate and bivariate multifractal spectra; univariate analysis for component 1 with $\log_2 L_{0,q}(j)$, $C_{10}(j)$ and $C_{20}(j)$ as functions of $\log_2 a$; univariate analysis for component 2 with $\log_2 L_{q,0}(j)$, $C_{01}(j)$ and $C_{02}(j)$ as functions of $\log_2 a$; bivariate analysis for components 1 and 2 with $\log_2 L_{q_1,q_2}(j)$, $\mathrm{Coh}^{(\mathrm{mf})}(j)$ and $C_{11}(j)$ as functions of $\log_2 a$.

Fig. 3 (second pair of rows) displays the same plots as above for another bi-MRW, with identical correlation as the first bi-MRW, but different joint statistics. Therefore, Fourier analysis and classical correlation analysis would not see any difference between these two bi-MRW, while bivariate multifractal analysis clearly does with different bivariate multifractal spectra (despite identical univariate multifractal spectra). Also, the wavelet leader multifractal coherence function $\mathrm{Coh}^{(\mathrm{mf})}(j)$ shows a constant, yet negative, value across scales, indicating temporal coincidences between the largest regularity exponents of one of the components and the smallest of the other components.

Finally, Fig. 3 (third pair of rows) uses an uncorrelated bi-MRW. In other words, Fourier analysis or classical correlation would not detect any correlation amongst the two components. By contrast, bivariate multifractal analysis clearly shows statistical dependencies beyond the second order. Indeed, the bivariate multifractal spectrum is the same as that of the first bi-MRW used in the top pair of rows, and so is the wavelet leader multifractal coherence function $\mathrm{Coh}^{(\mathrm{mf})}(j)$. This again indicates temporal coincidences of the largest or smallest regularity exponents within the two components.

4.5. Macroscopic brain activity: multifractal analysis

Univariate multifractal analysis has been used in the characterization of brain temporal dynamics. Notably, in [26], it was applied to MEG data to study infraslow brain activity, i.e. brain activity below 1 Hz (or across long time epochs, from 1 second to several tens of seconds). It showed that brain activity at rest was characterized by significant self-similarity (large H of the order of 0.9), with a significant occipital gradient, and low or no multifractality. This essentially means that the MEG time series representing brain activity at rest are characterized by a significant global correlation, which is larger in frontal regions than in occipital ones. It also means that this overall pattern is observed not to fluctuate locally over time, which indicates that brain activity at rest shows a constant over time, simple, and structured temporal dynamics. By contrast, La Rocca et al. [26] also show that task engagement yields a significant and overall decrease of self-similarity, yet increasing the fronto-occipital gradient: the decrease in self-similarity is more effective in the occipital regions (sensorial brain activity) of the brain than in the occipital ones (integrated/processing brain activities). This global decrease in self-similarity correlates with an increase of multifractality that remains, however, local and confined to regions of the brain that are involved in the task. Multifractality indicates bursty activity with significant fluctuations over time of the structures in brain activity: it can also be interpreted as fluctuations in the way time flows in the different part of the brain, compared to an overall brain clock [26].

Multivariate brain activity analysis remains to be conducted systematically over the whole brain and analyzed. Preliminary bivariate multifractal analysis, reported in Fig. 4, performed on the same two MEG brain activity signals used in Fig. 1 (bottom row), suggests multifractality in each component and reveals a non-trivial bivariate multifractal spectrum potentially indicating the modulation of higher-order statistical dependencies in brain from rest to task. These effects are under systematic analysis, and may permit to enrich the quantification of functional connectivity. While usually based on fMRI measurements and on correlation coefficients (hence static properties) between the corresponding time series, functional connectivity could also be investigated by exploiting the richer temporal dynamics available in MEG dynamics, by using the behaviors of wavelet and multifractal coherence functions with respect to time scales.

5. Conclusions and perspectives

Spectral estimation via Fourier transform (relying on a frequency translation operator) constitutes the classical cornerstone tool to assess cross-temporal dynamics in multivariate time series. When such dynamics are scale-free, i.e. not

governed by any particular scales of time playing a specific role, but rather by mechanisms that bind a large continuum of time scales together, spectral estimation can be efficiently and robustly conducted by means of the wavelet transform (multiscale, and relying on a dilation operator).

Beyond $1/f$ or power-law decreasing multivariate frequency spectra, multivariate scale-free dynamics can be better modeled by multivariate self-similarity. Multivariate wavelet eigenanalysis is based on a scale-by-scale wavelet decomposition of estimated wavelet coefficient covariance matrices. It provides an original, theoretically sound, and practically robust tool for assessing scale-free dynamics in multivariate temporal dynamics. Beyond the current theoretical analysis of estimation performance, several issues remain under investigation such as testing the number of different scaling exponents that actually exist amongst multivariate components [76], or addressing large-dimensional frameworks, when the number of components may be of the order of, or larger than, the number of time samples [77].

Furthermore, beyond the modeling of covariance, the characterization of scale-free dynamics may involve higher-order statistics. Therefore, multifractal analysis can be regarded as a further extension to multivariate Fourier analysis in the context of scale-free dynamics. It requires the use of multiscale representations constructed from nonlinear and non-local transforms of wavelet coefficients. It was recently shown that the extension from univariate to multivariate is not straightforward as the conditions under which the multivariate multifractal formalism yields the multivariate multifractal spectrum remain to be worked out (cf. [68] for an advanced discussion). However, preliminary work to be completed has illustrated that the multifractal spectrum conveys information related to the co-occurrences of singularities amongst components, and hence can, for some cases, be related to statistical dependencies amongst components that are not already encoded in covariance functions [72,73].

6. Acknowledgments

References

[1] A. Papoulis, Signal Analysis, vol. 191, McGraw-Hill, New York, 1977.
[2] T.W. Körner, Fourier Analysis, Cambridge University Press, 1988.
[3] B.G. Osgood, Lectures on the Fourier Transform and Its Applications, American Mathematical Society, Providence, RI, USA, 2019.
[4] P.J. Brockwell, R.A. Davis, Time Series: Theory and Methods, Springer Science and Business Media, 1991.
[5] J.W. Cooley, J.W. Tukey, An algorithm for the machine calculation of complex Fourier series, Math. Comput. 19 (90) (1965) 297–301.
[6] J.W. Cooley, The re-discovery of the fast Fourier transform algorithm, Mikrochim. Acta 93 (1–6) (1987) 33–45.
[7] G. Buzsáki, A. Draguhn, Neuronal oscillations in cortical networks, Science 304 (5679) (2004) 1926–1929.
[8] D. Veitch, P. Abry, A wavelet-based joint estimator of the parameters of long-range dependence, IEEE Trans. Inf. Theory 45 (3) (1999) 878–897.
[9] K. Park, W. Willinger, Self-similar network traffic: an overview, in: K. Park, W. Willinger (Eds.), Self-Similar Network Traffic and Performance Evaluation, Wiley, 2000, pp. 1–38.
[10] P. Abry, R. Baraniuk, P. Flandrin, R. Riedi, D. Veitch, Multiscale nature of network traffic, IEEE Signal Process. Mag. 19 (3) (2002) 28–46.
[11] R. Fontugne, P. Abry, K. Fukuda, D. Veitch, K. Cho, P. Borgnat, H. Wendt, Scaling in Internet traffic: a 14 year and 3 day longitudinal study, with multiscale analyses and random projections, IEEE/ACM Trans. Netw. 25 (4) (2017) 2152–2165.
[12] B. Mandelbrot, Information theory and psycholinguistics, in: B.B. Wolman, E. Nagel (Eds.), Scientific Psychology: Principles and Approaches, Basic Books, New York, 1965.
[13] L. Calvet, A. Fisher, B. Mandelbrot, The multifractal model of asset returns, in: Cowles Foundation Discussion Papers, vol. 1164, 1997.
[14] L. Calvet, A. Fisher, Multifractality in assets returns: theory and evidence, Rev. Econ. Stat. LXXXIV (84) (2002) 381–406.
[15] P. Frankhauser, L'approche fractale: un nouvel outil dans l'analyse spatiale des agglomerations urbaines, Population 4 (1997) 1005–1040.
[16] P. Abry, S. Jaffard, H. Wendt, When Van Gogh meets Mandelbrot: multifractal classification of painting's texture, Signal Process. 93 (3) (2013) 554–572.
[17] R. Leonarduzzi, P. Abry, S. Jaffard, H. Wendt, L. Gournay, T. Kyriacopoulou, C. Martineau, C. Martinez, p-Leader multifractal analysis for text type identification, in: Proc. 42nd IEEE International Conference on Acoustics, Speech and Signal Processing, ICASSP2017, New Orleans, LA, USA, 5–9 March 2017.
[18] L.S. Liebovitch, A.T. Todorov, Invited editorial on "Fractal dynamics of human gait: stability of long-range correlations in stride interval fluctuations", J. Appl. Physiol. (1996) 1446–1447.
[19] P.C. Ivanov, Scale-invariant aspects of cardiac dynamics, IEEE Eng. Med. Biol. Mag. 26 (6) (2007) 33–37.
[20] M. Doret, H. Helgason, P. Abry, P. Gonçalvès, Cl. Gharib, P. Gaucherand, Multifractal analysis of fetal heart rate variability in fetuses with and without severe acidosis during labor, Am. J. Perinatol. 28 (4) (2011) 259–266.
[21] T. Nakamura, K. Kiyono, H. Wendt, P. Abry, Y. Yamamoto, Multiscale analysis of intensive longitudinal biomedical signals and its clinical applications, Proc. IEEE 104 (2, SI) (2016) 242–261.
[22] H. Wendt, P. Abry, K. Kiyono, J. Hayano, E. Watanabe, Y. Yamamoto, Wavelet p-leader non Gaussian multiscale expansions for heart rate variability analysis in congestive heart failure patients, IEEE Trans. Biomed. Eng. 66 (1) (2019) 80–88.
[23] G. Werner, Fractals in the nervous system: conceptual implications for theoretical neuroscience, Front. Physiol. 1 (2010).
[24] B.J. He, Scale-free brain activity: past, present, and future, Trends Cogn. Sci. 18 (9) (2014) 480–487.
[25] B. Maniscalco, J.L. Lee, P. Abry, A. Lin, T. Holroyd, B.J. He, Neural integration of stimulus history underlies prediction for naturalistically evolving sequences, J. Neurosci. 38 (6) (2018) 1541–1557.
[26] D. La Rocca, N. Zilber, P. Abry, V. van Wassenhove, P. Ciuciu, Self-similarity and multifractality in human brain activity: a wavelet-based analysis of scale-free brain dynamics, J. Neurosci. Methods 309:175–187 (2018).
[27] U. Frisch, Turbulence, the Legacy of A.N. Kolmogorov, Addison-Wesley, 1993.
[28] D. Schertzer, S. Lovejoy, Physically based rain and cloud modeling by anisotropic, multiplicative turbulent cascades, J. Geophys. Res. 92 (1987) 9693–9714.

[29] B. Lashermes, S.G. Roux, P. Abry, S. Jaffard, Comprehensive multifractal analysis of turbulent velocity using the wavelet leaders, Eur. Phys. J. B 61 (2) (2008) 201–215.

[30] E. Foufoula-Georgiou, P. Kumar (Eds.), Wavelets in Geophysics, Academic Press, San Diego, CA, USA, 1994.

[31] S. Lovejoy, D. Schertzer, Scaling and multifractal fields in the solid Earth and topography, Nonlinear Process. Geophys. 14 (4) (2007) 465–502.

[32] B. Mandelbrot, W. Wallis, Noah, Joseph, and operational hydrology, Water Resour. Res. 4 (5) (1968) 909–918.

[33] B. Mandelbrot, The Fractal Geometry of Nature, 1982, New York.

[34] P. Abry, S. Jaffard, H. Wendt, Irregularities and scaling in signal and image processing: multifractal analysis, in: M. Frame, N. Cohen (Eds.), Benoît Mandelbrot: a Life in Many Dimensions, World Scientific Publishing, 2015, pp. 31–116.

[35] P. Ciuciu, P. Abry, B.J. He, Interplay between functional connectivity and scale-free dynamics in intrinsic fMRI networks, NeuroImage 95 (2014) 248–263.

[36] I. Daubechies, Ten Lectures on Wavelets, Society for Industrial and Applied Mathematics, Philadelphia, PA, USA, 1992.

[37] S. Mallat, A Wavelet Tour of Signal Processing, Academic Press, San Diego, CA, USA, 1998.

[38] P. Flandrin, On the spectrum of fractional Brownian motions, IEEE Trans. Inf. Theory IT-35 (1) (1989) 197–199.

[39] P. Flandrin, Wavelet analysis and synthesis of fractional Brownian motions, IEEE Trans. Inf. Theory 38 (1992) 910–917.

[40] P. Abry, P. Gonçalvès, P. Flandrin, Wavelets, spectrum estimation and $1/f$ processes, chapter 103 in: Wavelets and Statistics, in: Lecture Notes in Statistics, Springer-Verlag, New York, 1995.

[41] P. Abry, D. Veitch, Wavelet analysis of long-range dependent traffic, IEEE Trans. Inf. Theory 44 (1) (1998) 2–15.

[42] G. Didier, V. Pipiras, Integral representations and properties of operator fractional Brownian motions, Bernoulli 17 (1) (2011) 1–33.

[43] P. Abry, G. Didier, Wavelet estimation for operator fractional Brownian motion, Bernoulli 24 (2) (May 2018) 895–928.

[44] P. Abry, G. Didier, Wavelet eigenvalue regression for n-variate operator fractional Brownian motion, J. Multivar. Anal. 168 (2018) 75–104.

[45] C. Meneveau, K.R. Sreenivasan, P. Kailasnath, M.S. Fan, Joint multifractal measures – theory and applications to turbulence, Phys. Rev. A 41 (2) (1990) 894–913.

[46] S. Jaffard, S. Seuret, H. Wendt, R. Leonarduzzi, S. Roux, P. Abry, Multivariate multifractal analysis, Appl. Comput. Harmon. Anal. 46 (3) (2019) 653–663.

[47] P. Flandrin, Time-Frequency/Time-Scale Analysis, vol. 10, Academic Press, 1998.

[48] B. Whitcher, P. Guttorp, D.B. Percival, Wavelet analysis of covariance with application to atmospheric time series, J. Geophys. Res., Atmos. 105 (D11) (2000) 14941–14962.

[49] H. Wendt, G. Didier, S. Combrexelle, P. Abry, Multivariate Hadamard self-similarity: testing fractal connectivity, Physica D 356 (2017) 1–36.

[50] N. Zilber, P. Ciuciu, A. Gramfort, V. van Wassenhove, Supramodal processing optimizes visual perceptual learning and plasticity, Neuroimage 93 (Pt 1) (2014) 32–46.

[51] B. Mandelbrot, J.W. van Ness, Fractional Brownian motion, fractional noises and applications, SIAM Rev. 10 (1968) 422–437.

[52] G. Samorodnitsky, M. Taqqu, Stable Non-Gaussian Random Processes, Chapman and Hall, New York, 1994.

[53] M. Maejima, J.D. Mason, Operator-self-similar stable processes, Stoch. Process. Appl. 54 (1) (1994) 139–163.

[54] J.D. Mason, Y. Xiao, Sample path properties of operator-self-similar Gaussian random fields, Theory Probab. Appl. 46 (1) (2002) 58–78.

[55] G. Didier, V. Pipiras, Exponents, symmetry groups and classification of operator fractional Brownian motions, J. Theor. Probab. 25 (2) (2012) 353–395.

[56] C.-F. Chung, Sample means, sample autocovariances, and linear regression of stationary multivariate long memory processes, Econom. Theory 18 (2002) 51–78.

[57] H. Dai, Convergence in law to operator fractional Brownian motions, J. Theor. Probab. 26 (3) (2013) 676–696.

[58] P. Abry, G. Didier, H. Li, Two-step wavelet-based estimation for Gaussian mixed fractional processes, Stat. Inference Stoch. Process. 22 (2) (2019) 157–185.

[59] P.M. Robinson, Multiple local Whittle estimation in stationary systems, Ann. Stat. 36 (5) (2008) 2508–2530.

[60] S. Achard, D.S. Bassett, A. Meyer-Lindenberg, E. Bullmore, Fractal connectivity of long-memory networks, Phys. Rev. E 77 (3) (2008) 036104.

[61] D. La Rocca, P. Ciuciu, V. van Wassenhove, H. Wendt, P. Abry, R. Leonarduzzi, Scale-free functional connectivity analysis from source reconstructed MEG data, in: Proc. European Signal Processing Conference (EUSIPCO 2018), Rome, Italy, 3–7 September 2018.

[62] J. Frecon, G. Didier, N. Pustelnik, P. Abry, Non-linear wavelet regression and branch & bound optimization for the full identification of bivariate operator fractional Brownian motion, IEEE Trans. Signal Process. 64 (15) (2016) 4040–4049.

[63] R.H. Riedi, Multifractal processes, in: P. Doukhan, G. Oppenheim, M.S. Taqqu (Eds.), Theory and Applications of Long Range Dependence, Birkhäuser, 2003, pp. 625–717.

[64] S. Jaffard, Wavelet techniques in multifractal analysis, in: M. Lapidus, M. van Frankenhuijsen (Eds.), Fractal Geometry and Applications: a Jubilee of Benoît Mandelbrot, in: Proc. Symp. Pure Math., vol. 72(2), American Mathematical Society, Providence, RI, USA, 2004, pp. 91–152.

[65] H. Wendt, P. Abry, S. Jaffard, Bootstrap for empirical multifractal analysis, IEEE Signal Process. Mag. 24 (4) (2007) 38–48.

[66] S. Jaffard, C. Melot, R. Leonarduzzi, H. Wendt, P. Abry, S.G. Roux, M.E. Torres, p-exponent and p-leaders, part I: negative pointwise regularity, Physica A 448 (2016) 300–318.

[67] R. Leonarduzzi, H. Wendt, P. Abry, S. Jaffard, C. Melot, S.G. Roux, M.E. Torres, p-exponent and p-leaders, part II: multifractal analysis. Relations to detrended fluctuation analysis, Physica A 448 (2016) 319–339.

[68] D. Schertzer, S. Lovejoy, Physically based rain and cloud modeling by anisotropic, multiplicative turbulent cascades, J. Geophys. Res. 92.D8 (1987) 9693–9714.

[69] M. Ben Slimane, Baire typical results for mixed Hölder spectra on product of continuous Besov or oscillation spaces, Mediterr. J. Math. 13 (2016) 1513–1533.

[70] B. Castaing, Y. Gagne, M. Marchand, Log-similarity for turbulent flows, Physica D 68 (3–4) (1993) 387–400.

[71] A. Arneodo, E. Bacry, J.F. Muzy, The thermodynamics of fractals revisited with wavelets, Physica A 213 (1–2) (1995) 232–275.

[72] H. Wendt, R. Leonarduzzi, P. Abry, S. Roux, S. Jaffard, S. Seuret, Assessing cross-dependencies using bivariate multifractal analysis, in: 2018 IEEE International Conference on Acoustics, Speech and Signal Processing (ICASSP 2018), Calgary, Alberta, Canada, 15–20 April 2018.

[73] R. Leonarduzzi, P. Abry, S.G. Roux, H. Wendt, S. Jaffard, S. Seuret, Multifractal characterization for bivariate data, in: Proc. European Signal Processing Conference (EUSIPCO 2018), Rome, Italy, 3–7 September 2018.

[74] E. Bacry, J. Delour, J.F. Muzy, Multifractal random walk, Phys. Rev. E 64 (2) (2001) 026103.

[75] H. Helgason, V. Pipiras, P. Abry, Synthesis of multivariate stationary series with prescribed marginal distributions and covariance using circulant matrix embedding, Signal Process. 91 (2011) 1741–1758.

[76] H. Wendt, P. Abry, G. Didier, Wavelet domain bootstrap for testing the equality of bivariate self-similarity exponents, in: Proc. IEEE Workshop Statistical Signal Proces. (SSP), Freiburg, Germany, 10–13 June 2018.

[77] P. Abry, H. Wendt, G. Didier, Detecting and estimating multivariate self-similar sources in high-dimensional noisy mixtures, in: Proc. IEEE Workshop Statistical Signal Proces. (SSP), Freiburg, Germany, 10–13 June 2018.